EXPERIMENTAL EVALUATION OF

DRILL BIT TRANSVERSE VIBRATIONS

by

Ozan Tekinalp
Graduate Research Assistant

A. Galip Ulsoy
Assistant Professor

UM-MEAM-84-21

Center for Robotics and Integrated Manufacturing

and the

Department of Mechanical Engineering and Applied Mechanics

University of Michigan

Ann Arbor, Michigan 48109-2125

February 1984

1. Introduction

Billions of holes are drilled every year in the United States alone [1]. This makes the drilling process one of the most important machining operations. With increasing requirements on drilling accuracy and higher production rates, dynamic characteristics of the drill bits can no longer be neglected. The importance of transverse vibration and stability of drill bits for the precision of high speed drilling of small holes has already been emphasized by researchers [1-4].

Nevertheless drilling is probably the most complex machining process. Early researchers have spent substantial effort to understand drilling and to relate it to the orthogonal cutting process [5-8]. Modeling the drill point geometry is still one of the active research areas [9-11]. Drill wear [12-14], and drill point geometric optimization are still unresolved subjects.

Although there has been research about vibration in the metal cutting process, it has concentrated on the vibration of the machine tool itself. Chatter is a problem of the particular machine tool that arises at certain speeds and feeds [15,16]. Thus, it can be prevented by improving the design of the machine tool. However to prevent the vibration of the tool, the tool itself should be modeled. There are several papers published about the vibration, stability and control of band saw and circular saw blades [17-21]. Although there are researchers interesed in the transverse vibration and stability of drill bits, they do not consider the rotation of the drill [2,22-24]. The paper presented by Ulsoy [4] (see also appendix A) gives a lumped parameter model for drill bits and

1

investigates their transverse vibration.

The main formulas of Ulsoy's paper [4] will be presented here with reference to Appendix A. The drill bit is considered as a clamped-clamped massles rod with the mass lumped at the middle of the drill bit. Thus the total unsupported mass, (see figures A-la and A-lb)

$$m = \rho A(\ell - d) \tag{A-1}$$

and,

$$m\ddot{\underline{r}} = \Sigma\underline{f} = \underline{f}_e + \underline{f}_s + \underline{f}_d \tag{A-3}$$

where $\underline{r}$ is, the position vector; $\underline{f}_e$, $\underline{f}_s$, $\underline{f}_d$ are the external, spring and damping forces. Thus we have an overall equation,

$$\begin{bmatrix} m & 0 \\ 0 & m \end{bmatrix} \begin{Bmatrix} \ddot{x} \\ \ddot{y} \end{Bmatrix} + \begin{bmatrix} c_1 & -2m\Omega \\ 2m\Omega & c_1 \end{bmatrix} \begin{Bmatrix} \dot{x} \\ \dot{y} \end{Bmatrix} +$$

$$\begin{bmatrix} k_x - m\Omega^2 & -m\dot{\Omega} - c_2 \\ m\dot{\Omega} + \zeta\Omega & k_y - m\Omega^2 \end{bmatrix} \begin{Bmatrix} x \\ y \end{Bmatrix} = \begin{Bmatrix} f_x \\ f_y \end{Bmatrix} \tag{A-7}$$

where Ω, c_1, c_2 are rotational speed, and damping coefficients and k_x, k_y, f_x, f_y are stiffnesses and external forces in two transverse directions.

Before describing the various coeffcents in Eqn. (A-7) first consider the rotational speed $\Omega(t)$. From a control point of view one would like to maintain $\Omega(t)$ at a desired reference value. A typical controller torque T_c will be required to overcome the cutting torque T. Then a closed loop system which neglects the torsional stiffness and damping would be,

$$J\dot{\Omega} = T_c(t) - T \tag{1.1}$$

2

where J is the moment of inertia of the drill bit in the axial direction. A typical feedback controller for this rotational speed control application might be, e.g.,

$$T_c = k_1 \int_o^t (\Omega_r - \Omega) dt - k_2 \Omega \tag{1.2}$$

where k_1 and k_2 are controller gains selected to provide the desired performance characteristics.

In Eqn. (A-7) the damping effects are neglected, thus $c_1 = c_2 = 0$. The stiffness has two components arising from the clamped rod (k_{xo}, k_{yo}) and the thrust force employed during drilling (k_{x1}, k_{y1}). Thus,

$$k_x = k_{xo} + k_{x1}$$

$$\tag{A-8}$$

$$k_y = k_{yo} + k_{y1}$$

As discussed in Appendix A the total stiffnesses are,

$$k_x = \frac{192 EI_{xx}}{(\ell - d)^3} - \frac{4F_z}{(\ell - d)}$$

$$\tag{A-13}$$

$$k_y = \frac{192 EI_{yy}}{(\ell - d)^3} - \frac{4F_z}{(\ell - d)}$$

If the rotational speed is assumed to be constant, the damping coefficients are zero, and the stiffnesses are as given above, (A-7) becomes

$$\begin{bmatrix} m & 0 \\ 0 & m \end{bmatrix} \begin{Bmatrix} \ddot{x} \\ \ddot{y} \end{Bmatrix} + \begin{bmatrix} 0 & -2m\Omega \\ 2m\Omega & 0 \end{bmatrix} \begin{Bmatrix} \dot{x} \\ \dot{y} \end{Bmatrix} + \begin{bmatrix} k_x - m\Omega^2 & 0 \\ 0 & k_y - m\Omega^2 \end{bmatrix} \begin{Bmatrix} x \\ y \end{Bmatrix} = \begin{Bmatrix} f_x \\ f_y \end{Bmatrix} \tag{1-3}$$

3

If furthermore the stiffnesses in two transverse directions are assumed to be the same,

$$k_x = k_y = k \qquad (1.4)$$

and,

$$\omega_{n1} = \sqrt{k/m} \qquad (1.5)$$

where ω_{n1} is the fundamental transverse natural frequency, the characteristic equation obtained from (1.3) gives

$$\lambda_1 = (\omega_{n1} - \Omega)$$

$$(1.6)$$

$$\lambda_2 = (\omega_{n1} + \Omega)$$

If ω_{n1} is equal to the rotational speed of the drill bit (Ω), λ_1 vanishes. Thus the beam becomes very "soft" with zero stiffness. The fundamental natural frequency at zero speed may be defined as the critical rotational speed. Thus

$$\Omega_{cr} = \omega_{n1x} = \omega_{n1y} = \left(\frac{192EI}{\rho A(\ell-d)^4} - \frac{4F_z}{\rho A(\ell-d)^2} \right)^{1/2} \qquad (1.7)$$

where F_z is the thrust force; E the modulus of elasticity of the drill bit material; I is the transverse area moment of inertia, and A is the cross sectional area of the drill bit. If the drill bit is assumed to be a circular rod,

$$I = I_{xx} = I_{yy} = (\pi D^4/64)$$

$$(1.8)$$

$$A = (\pi D^2/4)$$

On the other hand if the fluted characteristic of the drill bit is considered from (A.33) and (A.34) we obtain,

$$I = I_{xx} = I_{yy} = 0.386 \ (\pi D^4/64)$$

$$(1.9)$$

$$A = 0.621 \ (\pi D^2/4)$$

In the discussion section of this report both forms, (1.8) and (1.9), of the drill bit moment of inertia and crossection are used to compare the zero speed fundamental natural frequency with the experimental results.

The thrust force F_z is dependent upon the drill diameter (D), feedrate (f) and Brinell hardness of the material (for torque/thrust formulas see Appendix B). Thus the model developed in [4] includes effects of drill rotational speed on feedrate as well as drill bit length, diameter and material properties. It shows that the transverse natural frequencies depend on the rotation speed, and transverse instability occurs at critical speeds where the natural frequencies vanish.

The purpose of this paper is to present the research initiated to validate the model developed by Ulsoy. The final goal of this research is to model the dynamics of drill bits accurately enough for control or design purposes. From this point of view the research reported here is considered to be a preliminary investigation that will enable us to outline future

research areas.

In sections two and three the experimental setup and the procedure respectively are discussed. Section four gives a discussion of the results. Appendix A is basically a review and extension of the theoretical relationships presented in [4], and gives the main formulas used for the lumped parameter model. Some torque and thrust formulas for drill bits, as developed by several researchers, are given in Appendix B.

2. Experimental Setup:

In order to study the dynamic characteristics of drill bits 6 different sizes of drills were used. They were at three different diameters: 6.35 mm (1/4 in), 4.7625 mm (3/16 in), 3.175 mm (1/8 in); and at two different lengths: 304.8 mm (12 in), 152.4 mm (6 in).

Obtaining sufficient information about the drilling process requires information about rotation speed, feed, torque, thrust and, transverse vibration. For this purpose the setup shown in Fig. 2.1 was utilized.

The drill press shown has a 2 hp motor and could be set to 4 different speeds (650, 1300, 1800, 3600; rpm) and to 4 different feeds (0.0381, 0.0762, 0.1524, 0.2286, 0.3048; mm/rev).

Torque and thrust measurements are taken by a torque/thrust dynamometer and recorded on a strip chart recorder via a 4 channel strain gage amplifier.

Transverse vibration is measured by two noncontacting proximity probes attached on two stands at two perpendicular directions. Probes give dc voltages (0/-18 volts) according to the transverse deflection of the drill bit via the proximeter. The signal taken from the proximeter is recorded on two channels of a 7 channel data recorder.

This recording is then replayed (gives 0.3v peak) and processed in the two channel spectrum analyzer. (Figures 2.2 and 2.3). It is very difficult if not impossible to process the vibration signal on line if one considers that at 0.1524 mm/rev and 3600 rpm, a drilling depth of 0.9 mm takes one second. On the other hand the spectrum analyzer needs one second to take one sample over a moderate (0 to 1 kHz) frequency range. The data

7

recorder provides the opportunity to process the data several times and at lower play back speeds.

The windowing used at the spectrum analyzer is uniform. Although uniform windowing doesn't give accurate measurements for amplitudes of the peaks, it is very accurate for the frequencies. The frequencies were particularly important in that the concern was to find out the damped natural frequencies of the system. The rms averaging method is used with different number of averages according to the condition of the signal.

3. Experimental Procedures

These experiments are designed to enable the data to be compared to the lumped parameter model. Thus the same procedure used in [4] is followed. However as indicated in the previous section there were constraints on the feed rate and rotational speed of the drill press used. On the other hand there are also physical constraints for the drilling process itself. Hence, while designing the experiments, it was attempted not to deviate significantly from recommended speeds and feeds given in [25].

The first set of experiments consisted of 8 drilling and 10 static tests. Drilling tests, feed, rotational speed, drill diameter and length are given in Table 4.1. These tests were designed to check torque and thrust formulas and to compare the critical rotational speed against feed, rotational speed, drill length and drill diameter. A piece of AISI 1112 annealed steel is drilled. This material is chosen because of its fairly brittle nature, to obtain broken chips during drilling which prevented the chips from rising along the flute and damaging the proximity probes hanging very close to the upper part of the drill. Some of the static tests were conducted to record the stand and drill press frequencies before the actual start of drilling. Other static tests were conducted to record the zero rotational speed fundamental frequency of the clamped-clamped and cantilever drill bit. The excitation during these static tests is applied by tapping on the particular structure.

During drilling we did not tap on the drill bit. It was expected that the cutting process would produce enough excitation on the drills to excite the drill natural frequencies. The basic drill length used was 152.4 mm (6 in). Having consumed 46 mm of

the length inside the chuck, the drill frequencies were in the range of 2000-5000 Hz. The cutting conditions were not sufficient to excite these frequencies. Thus, all the energy was consumed at stand and drill press frequencies (0-200 Hz).

Having experienced the above difficulties a second set of experiments were performed. This time long drills (304.8 mm) were used. The frequency range obtained was 100-400 Hz.

To get the transverse natural frequency vs. rotational speed curves (Fig. 4.3) actual drilling experiments were conducted with 6.35 mm diameter long drills at four different rotational speeds. Smaller diameters were also tried. However they easily became unstable and broke. This was not only because of the drop in the fundamental frequency but also due to the eccentricity inherent in the long drills.

For Fig. 4.4 two drilling experiment were conducted at 1300 rpm and at two different feeds. Higher feeds caused the chips to tangle on the probes hanging close to the drill bit. The feeds available on the drill press (see section 2) were not fine enough to obtain more experiments and stay below the recommended feeds in [25].

Figures 4.5 and 4.6 are the results of the static tests. Thus, the drills were loaded axially to the thrust force which would have been obtained during actual drilling, then excited by tapping on them while recording the probe output. The amount of the thrust force is checked by the dynamometer connected to the strain gage amplifier.

Analysis of the probe data as taken during actual drilling

introduces certain difficulties as emphasized before. During actual drilling the drill not only rotates but feeds axially. Thus the drill becomes stiffer as the drill proceeds inside the material. It is extremely important to know at what depth the drill is while taking the spectrum. Thus a trade off is faced. In order to get the best spectrum the tape recorder is slowed down three times. Thus the frequencies obtained were 1/3 of the actual frequencies. Then averaging is selected to be different for each rotational speed and feed, such that at the end of averaging the drill was approximately 12 mm inside the material. The error resulting from this procedure is discussed in the results section.

The signals obtained by static tests are analyzed at high averaging rates, namely 64 averages per spectrum. This not only gave an accurate averaging from the signal processing point of view but also helped to compensate for the probable damping introduced by tapping.

4. Results

In this section the results of the experiments will be given and the accuracy of the formulas will be discussed as they are introduced.

Table 4.1 gives the torque and thrust measurements and compares them with the formulas given by Boston and Oxford (see also Appendix B). In order to show the trends in these formulas they are plotted in Figs. 4.1 and 4.2.

Figure 4.1 gives the torque and thrust plots according to the change in feed. It can easily be seen that torque and thrust increases at higher feeds. It should be mentioned that the formulas given by Boston and Oxford are almost in 100% error when compared to each other. The experimental points are more or less scattered. For the case of torque, experimental points are closer to Boston's formula (see appendix B; Eqn. B-2). Boston's torque formula does not consider the drill point geometry and Brinell hardness of material as done by Oxford (Eqn. (B-3)). However the results do not seem to agree with those based on Oxford's formula. For the case of thrust the experimental points are close to Boston's second formula (Eqn. (B-4)). The other formula given by Boston (Eqn. (B-2)) is in error. Oxford's thrust formula (Eqn. (B-3)) is basically close to experimental points. However the shape of the curve given by Oxford's thrust formula conflicts with the one given by Boston's second formula (Eqn. (B-4)). For the case of torque the error inherited to the measurement is approximately $\pm$ 0.2 N-m. It is hoped that future experiments will be conducted using more sensitive bridge amplifiers.

Fig. 4.2 gives the torque and thrust readings vs. the drill

diameter. The two formula's given by Boston (Eqns. (B-2 and B-4)) and the one given by Oxford (Eqn. (B-3)) are also plotted. For the case of torque measurements they follow Boston's first formula (Eqn. (B-2)) very closely. For the case of thrust Oxford's formula (Eqn. (B-3)) is the closest one to experimental points. Oxford's (Eqn. (B-3)) and Boston's (Eqn. (B-2)) first thrust formulas show the same trend. Thus the thrust force increases as the drill diameter increases. However the second formula given by Boston (B-4) reverses this trend. Thus at 3.175 mm diameter it predicts a very high thrust force. This is mainly because of the weighing given to the web thickness (w) in this formula.

It should be mentioned that both Boston and Oxford conducted their experiments for drills bigger than 6.35 mm diameter. However the drills used in these experiments had smaller diameters. Both Boston and Oxford consider the (w/D) (web thickness/drill diameter) and (c/D) (chisel edge length/drill diameter) ratios to stay the same as the drill diameter increases. Unfortunately this is not the case for the drills used. In fact c/D increases from 0.194 to 0.28 and w/D increases from 0.156 to 0.224 as the drill diameter decreases from 6.35 mm to 3.175 mm (see Table B-1).

In the introduction (see also Appendix A) it was shown that the characteristic equation of the model (Eqn. (1.3)) will have two roots. At zero rotational speed these roots coincide. However when the rotational speed is increased the roots diverge from each other in a linear manner. Thus while one eigenvalue is

increasing the other one decreases and becomes zero when the rotational speed of the drill bit reaches the zero speed fundamental natural frequency. This rotational speed is called the critical rotational speed. Thus at critical rotational speed the rotating shaft will have a zero stiffness or in other words the rotating shaft becomes very "soft".

Fig. 4.3 shows the experimental points obtained for the fundamental natural frequencies of the drill bit at different rotational speeds. The figure also includes two theoretical predictions. The plot numbered (1) shows the model prediction by using a solid shaft (Eqn. (1.8)). Thus, the fluted geometry of the drill bit is neglected. The other plot (plot numbered as (2)) considers that the drill bit has a completely fluted geometry (Eqn. (1.9)). The solid shaft prediction gives higher frequencies. Thus it is stiffer than the fluted model. The experimental points are recorded when the drill is at 12 mm depth inside the material. In this case the 1/3 of the unsupported length was fluted while 2/3 of the drill had a round solid shape. It can be seen that the experimental points are between these two theoretical predictions and closer to the solid round shaft prediction as expected.

The zero rotational speed fundamental frequency is obtained statically by placing the drill inside the 12 mm hole and loading axially to the expected 755 N force. Then the drill bit is excited by tapping on it. The 650 rpm experiment results are not shown in the figure. The spectrum gave strong peaks around 270 to 280 Hz range. Some of these peaks were coming from the drill press. Thus, it was difficult to distinguish the actual drill bit

frequenices. The other points are taken at the available
rotational speeds possible on the drill press namely at 1300,
1800 and 3600 rpm.

Fig. 4.4 gives the fundamental natural frequencies taken at
1300 rpm and at two different feeds. The effect of increasing
the feedrate is to increase the thrust force. Thus at 0.0762
mm/rev the thrust force (F_z) is increased from 755N to 1100N.
The two models for solid shaft and fluted shaft are also ploted
in the figure. The drop in fundamental frequencies is slightly
higher for the fluted case than for the solid shaft prediction.
The fluted model employs the equivalent diameter which is smaller
than the shank diameter. Thus, for the fluted case the increase
in thrust force is much more pronounced than the solid shaft
case. The 0.0381 mm/rev experimental point agrees very well with
the solid shaft model. On the other hand the results of the
higher feedrate (0.0762 mm/rev), are closer to the fluted shaft
prediction. Although the model predicts the drop in natural
frequencies with increasing thrust forces the experimental points
seems to drop much more rapidly than the model predictions.
There may be several reasons for this drop. The averaging might
have introduced some error. Thus the higher feedrate case
resulted in fewer averages before the drill reached the 12 mm
depth. The eccentricity inherited from the drill bit might have
resulted the thrust force being more pronounced. Finally the
frequencies arising from the stands and the drill press might
have shifted the actual drill bit peaks. Nevertheless these
results are between two theoretical model predictions.

15

In Fig. 4.5 the fundamental natural frequencies at zero rotational speed vs. drill diameter are shown where depth is a parameter. Experimental points are collected at two different depths and three different diameters. The two model predictions (solid and fluted models) are also ploted for comparison. These experimental points are obtained by placing the drills into the holes at two different depths and loading them axially to the expected thrust forces.

The experimental points lie closer to the solid model as expected. There are two points at the middle of the two model predictions. These are the ones with 4.76 mm diameter at 5 mm depth and 6.35 mm diameter at 40 mm depth. The model is developed with the assumption that the drill has built in support conditions, while the actual conditions probably lie between the clamped-clamped and the clamped hinged cases. Also the static tests apply only the thrust force. However during actual drilling drill is also loaded with torque. Although not included in this model, this load is coupled to the transverse vibration of the drill bit. Note also that the model predicts divergence buckling ($\omega_{n1}=0$) for small drill diameters. The experimental points are not too far from the model predictions and follow the trends quite closely.

The change in drill fundamental frequencies at two different lengths and depths are shown in Fig. 4-6. The figure includes two model predictions and the experimental points obtained. It can easily be seen that at both depths the experimental points lie between the two model predictions and close to the solid shaft model.

16

The experimental results presented above are in good
agreement with the two models. The solid shaft model assumes
that the drill bit has a solid round crossection. The fluted
model uses the idea of effective diameter to calculate the
crossectional area and area moment of inertia of the drill bit.
The drill bits used had a fluted crossection along 1/3rd of it's
unsupported length. The experimental points obtained lie between
these two models closer to the solid shaft model as expected.
Thus, the experimental points represent an overall error of less
than 20% when compared to any of the models.

5. Conclusion

In this report, the experiments conducted to investigate the accuracy of the lumped parameter model in [4] are presented. The results given in section four are in good agreement with one of the versions of the model. The overall error of the results when compared with any two versions of the model is less than 20%. This error is better than expected considering the possible errors in the experiments and the assumptions made during the derivation of the model (see Appendix A).

It can be said that the lumped parameter model [4] can easily be used for control purposes after small modifications. Thus, it is hoped to develop a better model in the future by the experience gained during this preliminary investigation.

One of the extension that will be investigated is to model the torsional vibration which is probably coupled with the transverse vibration. The final step is nevertheless to develop a distributed parameter model that will at least include transverse and torsional vibration of the drill bit. Then using the models obtained, a simpler version to be used for control purposes will be derived.

The importance of the vibration and stability of the drill bits for high speed precision drilling requires research on the dynamic characteristics of the drill bits. The research initiated here to investigate the dynamic characteristics of drill bits will enable us to improve the accuracy of the drilling operation.

6. Acknowledgements

Appendix A

A Lumped Parameter Model for the Transverse Vibration of Drill Bits.

A lumped parameter model for the transverse vibration of drill bits has been developed by Ulsoy [4]. It will be presented here briefly including some extensions which consider the concepts of effective mass and effective stiffness.

With reference to Fig. A-1a and Fig. A-1b; the total unsupported mass, of the drill is,

$$m = \rho A(\ell-d) \tag{A-1}$$

The position vector,

$$\underline{r} = x\ \underline{e}_x + x\ \underline{e}_y \tag{A-2}$$

from Newton's second law,

$$m\underline{\ddot{r}} = \Sigma\underline{f} = \underline{f}_e + \underline{f}_s + \underline{f}_d \tag{A-3}$$

$$\underline{f}_e = f_x\ \underline{e}_x + f_y\ \underline{e}_y \tag{A-4}$$

$$\underline{f}_s = -k_x\ x\ \underline{e}_x - k_y\ y\ \underline{e}_y \tag{A-5}$$

$$\underline{f}_d = -(c_1\dot{x} - c_2\Omega y)\underline{e}_x - (c_1\dot{y} + c_2\Omega x)\underline{e}_y \tag{A-6}$$

where $\underline{f}_e$ are external forces, $\underline{f}_s$ are stiffness forces, and, f_d are damping forces. The above relationships give an overall equation,

$$\begin{bmatrix} m & o \\ o & m \end{bmatrix} \begin{Bmatrix} \ddot{x} \\ \ddot{y} \end{Bmatrix} + \begin{bmatrix} c_1 & -2m\Omega \\ 2m\Omega & c_1 \end{bmatrix} \begin{Bmatrix} \dot{x} \\ \dot{y} \end{Bmatrix} +$$

$$\begin{bmatrix} k_x - m\Omega^2 & -m\dot{\Omega} - c_2\Omega \\ m\dot{\Omega} + c_2\Omega & k_y - m\Omega^2 \end{bmatrix} \begin{Bmatrix} x \\ y \end{Bmatrix} = \begin{Bmatrix} f_x \\ f_y \end{Bmatrix} \qquad \text{(A-7)}$$

In the above equation c_1, c_2 are damping coefficients [4]. They should be determined by experimental methods and are open to extensive research. For the time being c_1 and c_2 will be considered zero.

Next we consider the modeling of the transverse stiffness of the drill bit. A drill bit inside the material at depth $d > 0$ may be considered as a massless clamped-clamped rod with its mass lumped at the middle of the rod. (Fig. A-2). In this case the stiffness will have two components,

$$k_x = k_{xo} + k_{x1}$$

$$\text{(A-8)}$$

$$k_y = k_{yo} + k_{y1}$$

Where k_{xo} is the stiffness of the clamped-clamped beam and k_{x1} is the additional parameter resulting from the thrust force encountered in the drilling process.

Shigley [26] gives the deflection of a clamped-clamped beam loaded at the middle,

$$y_{max} = \frac{F_x \ell^3}{192EI_{xx}} \qquad \text{(A-9)}$$

Thus, the stiffness can be written as,

$$k_{xo} = \frac{192EI_{xx}}{(\ell-d)^3}$$

$$\text{(A-10)}$$

$$k_{yo} = \frac{192EI_{yy}}{(\ell-d)^3}$$

With reference to Fig. A-3 a x length transverse deflected rod creates a reaction force,

$$F_x = 2F_z \sin\theta \approx 2F_z\theta \approx 2F_z(x/(\ell-d)/2) \qquad (A-11)$$

Here the deflection of rod is assumed to be negligible compared with the free length of the drill. Thus, is a small angle. From Eqn. (A-11) the stiffness arising from the thrust force F_z is,

$$k_{x1} = 4F_z/(\ell-d)$$

$$(A-12)$$

$$k_{y1} = 4F_z/(\ell-d)$$

Emprical relations for F_z are given in Appendix B. Thus,

$$k_x = k_{xo} + k_{x1} = \frac{192EI_{xx}}{(\ell-d)^3} - \frac{4F_z}{(\ell-d)}$$

$$(A-13)$$

$$k_y = k_{yo} + k_{y1} = \frac{192EI_{yy}}{(\ell-d)^3} - \frac{4F_z}{(\ell-d)}$$

Here F_z is the thrust force which acts as a reducer of stiffness. Dividing the stiffness by the total mass of the rod (the mass that is lumped), gives the fundamental natural frequencies in two directions.

$$\omega_{nx1} = \sqrt{\frac{k_x}{m}} = \left(\frac{k_x}{\rho A(\ell-d)}\right)^{1/2} = \left(\frac{192EI_{xx}}{\rho A(\ell-d)^4} - \frac{4F_z}{\rho A(\ell-d)^2}\right)^{1/2}$$

$$\omega_{ny1} = \sqrt{\frac{k_y}{m}} = \left(\frac{k_y}{\rho A(\ell-d)}\right)^{1/2} = \left(\frac{192EI_{yy}}{\rho A(\ell-d)^4} - \frac{4F_z}{\rho A(\ell-d)^2}\right)^{1/2}$$

Another way to obtain a lumped parameter model of a system

is to use the idea of equivalent mass. This can be realized by equating the kinetic energies of the lumped and distributed systems as proposed by Palm [27].

With reference to Fig. A-4, the kinetic energy of the clamped-clamped beam vibrating at its first natural frequency is [28],

$$KE = \frac{1}{2} \mu_1 \omega_{n1}^2 \int_0^{(\ell-d)} y^2 dz$$

$$(A-15)$$

$$\mu_1 = m/(\ell-d)$$

Fig. A-4 gives the approximate first mode shape [28]. Thus, employing this equation gives,

$$KE = \frac{3}{4} y_o^2 \omega_{n1}^2 m \qquad (A-16)$$

The Kinetic Energy of the system with equivalent mass is,

$$KE = \frac{1}{2} m_e \omega_{n1}^2 (2y_o)^2 \qquad (A-17)$$

These two expressions for KE should be equal as proposed. Thus,

$$m_e = 0.375 \, m \qquad (A-18)$$

Now we can get the fundamental frequencies by using the stiffness expressions given previously in Eqns. (A-10) and (A-11)

$$\omega_{n1xo}^2 = \frac{192EI_{xx}}{(\ell-d)^3 m_e} = \frac{512EI_{xx}}{\rho A (\ell-d)^4}$$

$$(A-19)$$

$$\omega_{n1yo}^2 = \frac{192EI_{yy}}{(\ell-d)^3 m_e} = \frac{512EI_{yy}}{\rho A (\ell-d)^4}$$

23

$$\omega_{n1x1}^2 = \omega_{n1y1}^2 = \frac{4F_z}{(\ell-d)m_e} = \frac{10.66\ F_z}{\rho A(\ell-d)^2} \qquad \text{(A-20)}$$

Thus, the fundamental natural frequencies are,

$$\omega_{n1x1} = \left(\frac{512EI_{xx}}{A(\ell-d)^4} - \frac{10.66\ F_z}{A(\ell-d)^2}\right)^{1/2}$$

(A-21)

$$\omega_{n1y1} = \left(\frac{512EI_{yy}}{\rho A(\ell-d)^4} - \frac{10.66\ F_z}{\rho A(\ell-d)^2}\right)^{1/2}$$

Another approach for obtaining a lumped parameter model of the system is to equate the fundamental frequencies of the lumped and distributed systems.

The fundamental frequency of a clamped-clamped beam is,

$$\omega_{n1xo}^2 = (22.4)^2 EI/(m(\ell-d)^3) \qquad \text{(A-22)}$$

Thus,

$$k_{eqxo} = 501.75\ EI_{xx}/(\ell-d)^3$$

(A-23)

$$k_{eqyo} = 501.75\ EI_{yy}/(\ell-d)^3$$

In order to find the equivalent stiffness of the massless rod that is subjected to a thrust force we can assume that the cross section of the rod is small and consider the rod to be a

string. With reference to Fig. A-5 [29],

$$\omega_{n1x1} = \omega_{n1y1} = \pi^2 F_z/(\rho(\ell-d))^2 \qquad \text{(A-24)}$$

and the first natural frequency of the lumped system is,

$$\omega_{n1x1} = \omega_{n1y1} = k_{eqx1}/m \qquad \text{(A-25)}$$

Thus,

$$k_{eqx1} = \pi^2 F_z/(\ell-d)$$

$$\qquad \text{(A-26)}$$

$$k_{eqy1} = \pi^2 F_z/(\ell-d)$$

Using the equivalent stiffness given by Eqns. (A-23), (A-26) and the assumption in Eqn. (A-8)

$$k_{eqx} = \frac{501.75EI_{xx}}{(\ell-d)^3} - \frac{\pi^2 F_z}{(\ell-d)}$$

$$\qquad \text{(A-27)}$$

$$k_{eqy} = \frac{501.75EI_{yy}}{(\ell-d)^3} - \frac{\pi^2 F_z}{(\ell-d)}$$

Thus, the first natural frequency, using the equivalent

stiffnesses in Eqn. (A-28) and the total mass m, can be expressed

as

$$\omega_{n1x} = \sqrt{\frac{k_{eqx}}{m}}$$

$$\qquad \text{(A-28)}$$

$$\omega_{n1y} = \sqrt{\frac{k_{eqy}}{m}}$$

$$\omega_{n1x} = (\frac{501.75EI_{xx}}{\rho A(\ell-d)^4} - \frac{\pi^2 F_z}{\rho A(\ell-d)^2})^{1/2}$$

$$\omega_{nly} = \left(\frac{501.75EI_{yy}}{\rho A(\ell-d)^4} - \frac{\pi^2 F_z}{\rho A(\ell-d)^2}\right)^{1/2} \tag{A-29}$$

or,

$$\omega_{nlx} = \left(\frac{501.75EI_{xx}}{\rho A(\ell-d)^4} - \frac{9.87F_z}{\rho A(\ell-d)^2}\right)^{1/2}$$

$$\omega_{nly} = \left(\frac{501.75EI_{yy}}{\rho A(\ell-d)^4} - \frac{9.87F_z}{\rho A(\ell-d)^2}\right)^{1/2} \tag{A-30}$$

Now we can compare the two lumped models given in Eqns. (A-21) and (A-30) which were developed by using the idea of equivalent mass and equivalent stiffness respectively.

These two sets of equations have the same form, namely

$$\omega_{nl} = \left(\frac{\alpha EI}{\rho A(\ell-d)^4} - \frac{\beta F_z}{\rho A(\ell-d)^2}\right)^{1/2} \tag{A-31}$$

The coefficient α given in Eqn. (A-30) is 2% higher than the one given in Eqn. (A-21). This basically arises from the approximation made for the first mode shape of the clamped-clamped beam in Fig. A-4. The second coefficients in Eqn. (A-30) is 8% lower then the one found in Eqn. (A-21). This not only arises from the assumptions made regarding the massless rod and string but also the assumption made regarding the first mode shape.

The coefficients described by Eqn. (A-31) are given in Table A-1 for Eqns. (A-14), (A-21) and (A-30).

In order to complete the model development we must know the moment of inertia and crossectional area of the drill bit. Although flute geometry changes from one manufacturer to another,

the approximate values given by Burnham [2] are quite reasonable and will be employed.

Thus,

$$D_e = 0.788D \qquad (A-32)$$

where D_e is the effective drill diameter for the calculation of mass moement of inertia and crossectional area for the fluted part of the drill. D is the diameter of the solid part of the drill. Hence,

$$A = \pi(0.788D/2)^2 = (0.621)(\pi D^2/4) \qquad (A-33)$$

$$I = I_{xx} = I_{yy} = (0.386)(\pi D^4/64) \qquad (A-34)$$

The values used for the calculation of the theoretical first natural frequency for a particular experiment are given in Table A-2.

Table A-3 gives the comparison between an experimental point with the three theoretical formulations. From the table it can be seen that the difference in the last two columns is less then 0.5% as opposed to the differences between the two coefficients given in Table A-1, where it was 8%. This is the result of the low thrust forces employed in the experiment.

Having modeled the transverse stiffness and fundamental natural frequency of the drill bit we can reconsider Eqn. (A-7). Assume that the drilling is done at constant rotational speed and that the damping coefficents are zero:

$$\dot{\Omega} = 0,$$

$$c_1 = c_2 = 0 \qquad\qquad (A-35)$$

Also assume that the stiffnesses in the two transverse directions are equal,

$$k_x = k_y = k \qquad\qquad (A-36)$$

Then Eqn. (A-7) becomes:

$$\begin{bmatrix} m & o \\ o & m \end{bmatrix} \begin{Bmatrix} \ddot{x} \\ \ddot{y} \end{Bmatrix} + \begin{bmatrix} o & -2m\Omega \\ 2m\Omega & o \end{bmatrix} \begin{Bmatrix} \dot{x} \\ \dot{y} \end{Bmatrix} + \begin{bmatrix} k_x - m\Omega^2 & o \\ o & k_y - m\Omega^2 \end{bmatrix} \begin{Bmatrix} x \\ y \end{Bmatrix} = \begin{Bmatrix} f_x \\ f_y \end{Bmatrix}$$

$$(A-37)$$

Solving the characteristic equation of this sytem gives

$$\lambda_1 = (\omega_{n1} - \Omega)$$

$$(A-38)$$

$$\lambda_2 = (\omega_{n1} + \Omega)$$

Assume, $\omega_{n1} = \Omega$. Thus,

$$\lambda_1 = 0$$

$$(A-39)$$

$$\lambda_2 = 2\Omega$$

which simply means that the stiffness of the drill bit is zero. Hence it can easily deflect with any external force. We may rename the zero rotational speed fundamental natural frequency of drill bit as a critical rotational speed (Ω_{cr}). When the rotation of the drill bit reaches this speed the drill bit becomes very "soft" or even unstable. In reality there is a slight difference between the two transverse direction stiffnesses of the drill bit. Thus Ω_{cr} occupies a region, namely

28

$$\sqrt{k_y/m} < \Omega_{cr} < \sqrt{k_x/m} \qquad\qquad\qquad \text{(A-40)}$$

$$k_x > k_m$$

Eqn. (A-39) also shows that the fundamental natural frequency of a drill bit will split into two as the rotational speed is increased. Typical plots for this phenomenon are given in Fig. 4.3.

Appendix B

Torque and Thrust Formulas for Drill Bits

There has been several formulas proposed by researchers
[5-9]. These formulas are all developed emprically from various
experimental data. They are generally of the form,

$$F_z = C f^{\gamma} D^{\delta}$$

$$T = K f^{\xi} D^{\eta}$$

(B-1)

where f and D are the feed and drill diameter respectively and C,
γ, δ, K, ξ, η are the constants related to the drill geometry and
the material to be drilled. Boston and Oxford have related these
constants to the Brinell hardness of the material.

The formulas proposed by Boston [5] are

$$F_z = C_1 f^{0.78} D$$

$$T = K_1 f^{0.78} D^{1.8}$$

(B-2)

where K_1 and C_1 are related to the Brinell hardness of the
workpiece used.

Shaw and Oxford applied dimensional analysis to drilling and
showed that torque and thrust are not only dependent on the
Brinell hardness of the material, but also the chiesel edge
thickness (c) of the drill point. Typical formulas as given by
Shaw and Oxford in [8] are,

$$\frac{F_z}{D^2 H_b} = \frac{C_2 f^{0.78}}{D^{1.2}} \left[\frac{(1-\frac{c}{D})}{(1+\frac{c}{D})} + 2.2 \left(\frac{c}{D}\right)^{0.8} \right] + C_3 \left(\frac{c}{D}\right)^2$$

(B-3)

$$\frac{T}{D^3 H_b} = \frac{K_2 f^{0.8}}{D^{1.2}} \left[\frac{(1-\frac{c}{D})}{(1+\frac{c}{D})} + 3.2 (\frac{c}{D})^{1.8} \right]$$

where c is the chiesel edge thickness of the drill point. The ratio c/D changed from 0.194 to 0.280 for the drill bits used according to the drill diameter. Hence employing these values reduces the complexity of the formulas considerably.

Similar formulas given by Boston [5] are,

$$F_z = C_4 f^{0.87} (\frac{D}{127} + \frac{w}{D})^{2.12}$$

(B-4)

$$T = K_4 f^{0.78} D^{1.8}$$

where w is the web thickness of the chiesel edge and K_4 and C_4 are again related to the Brinell hardness of the workpiece.

The most detailed formulas which relate the complete drill point geometry and material properties are the ones given by Williams [9]. Williams divides the drill point into three regions: Main cutting edge, secondary cutting edge, and the indentation zone. He then develops semianalytical formulas for these three regions. Although they are very detailed and probably accurate, their use requires detailed information about the drill point geometry. It is not only difficult to obtain the complete drill point geometry from the manufacturer or by measuring it, but also difficult to get two identical drills in the market. Thus, these formulas are not utilized in this study, considering the fact that 5% error in torque and thrust measurements were acceptable for the purposes of this research.

Table B-1 gives the drill point dimensions of the drills

used. These are taken by using a tool microscope which is accurate to one thousands of an inch.

Table B-2 gives the constant used for the AISI 1112 steel. These values are obtained from [5,8].

References

1. Khang, C.H., "Research Goals in High Speed Drilling", SME Paper No. MR77-348, 1977.

2. Burnham, M.W., "The Mechanics of Drilling Small Holes", 10th North American Manufacturing Research Conference, Ontario, May 1983.

3. Burnham, M.W. "An Analysis of Drill Deflection for Deep Miniature Holes". SME Paper No. MR80-956, 1980.

4. Ulsoy, A.G., "A Lumped Parameter Model for the Transverse Vibration of Drill Bits", In Hardt D.E. and W.J. Book (eds), Control of Manufacturing Process and Robotic Systems, ASME, 1983, pp. 15-26.

5. Boston, O.W., Metal Processing, 2nd ed., John Wiley and Sons, London, 1951.

6. Galloway, D.F., "Some Experiments on the Influence of Various Factors on Drill Performance", ASME Transactions, July 1957, vol. 77, pp. 191-230.

7. Oxford, C.J. Jr., "On the Drilling of Metals - I Basic Mechanics of the Process", ASME Transactions vol. 77, Feb. 1955, pp. 103-114.

8. Shaw, M.C. and C.J. Oxford Jr., "On the Drilling of Metals". ASME Transactions, vol. 79, Jan. 1957.

9. Williams, R.A., "A Study of the Drilling Process", Journal of Engineering for Industry, Nov. 1974, pp. 1207-1215.

10. Wu, S.M. and J.U. Shen, "Mathematical Model for Multi-facet Drills", Journal of Engineering for Industry, vol. 105, August 1983, pp. 180-183.

11. Fugelso, M.A., "Cylindrical Flank Twist Drill Points", ASME Journal of Engineering for Industry, vol. 105, August 1983, pp. 183-186.

12. Kaldor S. and E. Lenz, Investigation in Tool Life of Twist Drills, Technion Israel Institute of Technology, Hafia.

13. Lenz, E., Mayer J.E. and D.G. Lee, "Investigation in Drilling", Technion Israel Institute of Technology - Hafia, Israel, Machining and Wear Department, Ford Motor Co., U.S.A.

14. Kaldor, S. and E. Lenz, "Drill Point Geometry and Optimization", ASME Journal of Engineering for Industry, vol. 105, February 1982, pp. 173-182.

15. Armerego, E.J.A., Brown, R.H., The Machining of Metals, 1st ed. Prentice Hall, Englewood Cliffs, N.J., 1969.

D (mm)	c (mm)	w (mm)	c/D	w/D
6.350	1.232	.991	.194	.156
4.763	.965	.782	.203	.164
3.175	.889	.711	.280	.224

Table B-1   Drill diameter (D), chiesel edge (c), web thickness (w), average values for the drills used.

K_1	0.393
K_2	0.0029251
C_1	432.23
C_2	5.351
C_3	0.66512
C_4	166244.

Table B-2   Constants used for torque thrust formulas for AISI 1112 steel.

16. Tobias, S.A., <u>Machine Tool Vibration</u>, John Wiley and Sons, Inc., 1965, NY.

17. Mote, C.D., Jr. and R. Szymari, "Circular Saw Vibration Research", <u>Shock and Vibration Digest</u>, vol. 10, no. 61, 1978, pp. 15-30.

18. Radcliffe, C.J., Mote, C.D. Jr., "Identification and Control of Rotating Disk Vibration", <u>ASME Journal of Dynamic Systems, Measurement and Control</u>, vol. 105, no. 1, March 1983, pp. 39-45.

19. Ulsoy, A.G. and C.D. Mote Jr., "Band Saw Vibration and Stability", <u>Shock and Vibration Digest</u>, vol. 10, no. 11, 1978, pp. 3-15.

20. Ulsoy, A.G., and C.D. Mote, Jr., "Vibration of Wide Band Saw Blades", <u>ASME Journal of Engineering for Industry</u>, vol. 104, no. 1, Feb. 1982, pp. 71-78.

21. Ulsoy, A.G., "Vibration Control in Rotating and Translating Elastic Systems", <u>ASME Journal of Dynamic Systems, Measurement, and Control</u>, March 1984.

22. Dawson, B. and W. Carnegie, "Modal Curves of Pre-Twisted Beams of Rectangular Cross-Section", <u>ASME Journal of Engineering for Industry</u>, August 1970.

23. Kar, R.C., W. Hanger, "Stability of Pretwisted Tapered Centilever Beam Subjected to Dissipative and Follower Forces", <u>Journal of Sound and Vibration</u>, vol. 81, no. 4, 1982, pp. 565-573.

24. Subrahmanuam, K.B., and T.J. Rao, "Coupled Bending and Bending Vibrations of Tapered Centilever Beams Treated by Reissner Method", <u>Journal of Sound and Vibration</u>, vol. 82, no. 4, 1982, pp. 577-592.

25. Kronenberg, M., <u>Drilling Feeds</u>, Machinery, London, 45, 1935.

26. Shigley, J.E., <u>Mechanical Engineering Design</u>, 3rd ed. McGraw Hill, Tokyo, 1977.

27. Palm, William J. III, <u>Modeling, Analysis and Control of Dynamic Systems</u>, 1st ed., John Wiley and Sons, NY, 1983.

28. Den Hartog, J.P., <u>Mechanical Vibrations</u>, 2nd ed. Mc-Graw Hill, New York, 1940.

29. Thomson, William T., <u>Theory of Vibration with Applications</u>, pp. 210-211, 2nd ed., Prentice Hall Inc., Englewood Cliffs, N.J., 1981.

Sons, Inc., 1965, NY.

17. Mote, C.D., Jr. and R. Szymari, "Circular Saw Vibration
     Research", Shock and Vibration Digest, vol. 10, no. 61,
     1978, pp. 15-30.

18. Radcliffe, C.J., Mote, C.D. Jr., "Identification and
     Control of Rotating Disk Vibration", ASME Journal of
     Dynamic Systems, Measurement and Control, vol. 105, no.
     1, March 1983, pp. 39-45.

19. Ulsoy, A.G. and C.D. Mote Jr., "Band Saw Vibration and
     Stability", Shock and Vibration Digest, vol. 10, no. 11,
     1978, pp. 3-15.

20. Ulsoy, A.G., and C.D. Mote, Jr., "Vibration of Wide Band
     Saw Blades", ASME Journal of Engineering for Industry,
     vol. 104, no. 1, Feb. 1982, pp. 71-78.

21. Ulsoy, A.G., "Vibration Control in Rotating and Translating
     Elastic Systems", ASME Journal of Dynamic Systems,
     Measurement, and Control, March 1984.

22. Dawson, B. and W. Carnegie, "Modal Curves of Pre-Twisted
     Beams of Rectangular Cross-Section", ASME Journal of
     Engineering for Industry, August 1970.

23. Kar, R.C., W. Hanger, "Stability of Pretwisted Tapered
     Centilever Beam Subjected to Dissipative and Follower
     Forces", Journal of Sound and Vibration, vol. 81, no.
     4, 1982, pp. 565-573.

24. Subrahmanuam, K.B., and T.J. Rao, "Coupled Bending and
     Bending Vibrations of Tapered Centilever Beams Treated
     by Reissner Method", Journal of Sound and Vibration,
     vol. 82, no. 4, 1982, pp. 577-592.

25. Kronenberg, M., Drilling Feeds, Machinery, London,
     45, 1935.

26. Shigley, J.E., Mechanical Engineering Design, 3rd ed.
     McGraw Hill, Tokyo, 1977.

27. Palm, William J. III, Modeling, Analysis and Control of
     Dynamic Systems, 1st ed., John Wiley and Sons, NY, 1983.

28. Den Hartog, J.P., Mechanical Vibrations, 2nd ed.
     Mc-Graw Hill, New York, 1940.

29. Thomson, William T., Theory of Vibration with Applications,
     pp. 210-211, 2nd ed., Prentice Hall Inc., Englewood Cliffs,
     N.J., 1981.

Nomenclature

A	crossection area of drill bit
c_1, c_2	coefficients of viscous damping
C_1, C_2, C_3, C_4	emprical coefficients for thrust force
c	chisel edge length of drill bit
d	depth of hole
D	drill diameter
$\underline{e}_x, \underline{e}_y$	unit vectors of rotating coordinate system
E	modulus of elasticity of the drill bit
f	feed
f_x, f_y, f_z	transverse and axial forces on the drill bit
F_z	thrust force
$\underline{i}, \underline{j}$	unit vectors of the fixed coordinate system
I_{xx}, I_{yy}	area moment of inertia about the x and y axis respectively
k_x, k_y	transverse stiffness coefficients in x and y directions
K_1, K_2, K_4	empirical coefficient for torque
k_1, k_2	controller gains for feedback controller
k_{ex}, k_{ey}	effective stiffness of the drill bit in x and y direction
ℓ	drill length
m	lumped mass of the drill bit
m_e	effective lumped mass of the drill bit.
T	torque
w	web thickness of drill point
x, y	drill transverse deflections in rotating coordinate system
α, β	coefficients for fundamental natural frequency formulation

35

$\gamma, \delta, \xi, \eta$ exponents used in the emprical relationships defining torque and thrust force

ρ mass density of the drill material

Ω drill rotational speed

Ω_{cr} critical rotational speed

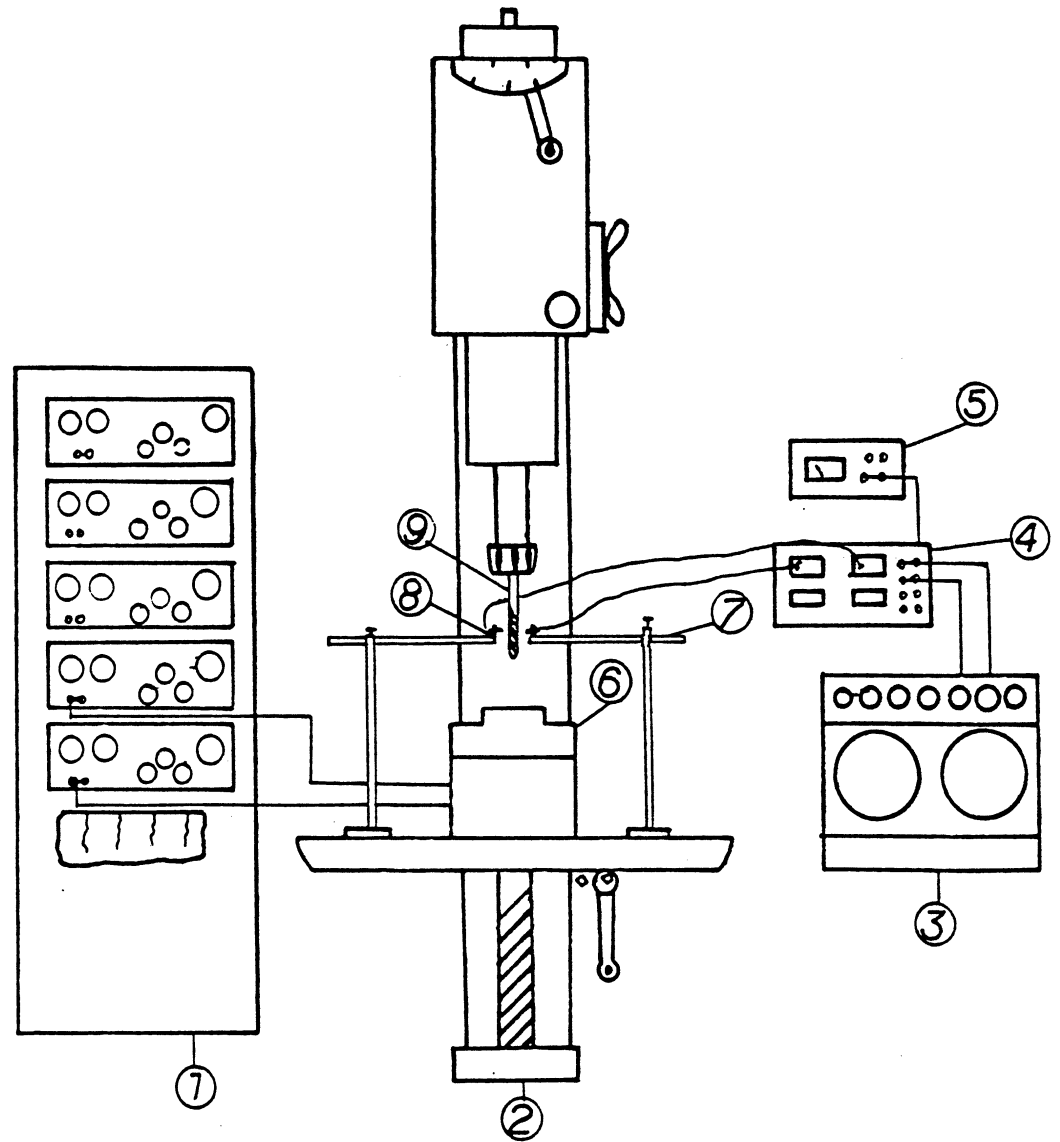Ω_r reference rotational speed value

Fig. 2.1   Experimental Setup

(1)   Strain gage amplifier

(2)   Drill press

(3)   Data Recorder

(4)   Proximitor

(5)   Power supply

(6)   Torque, Thrust dynamometer

(7)   Stands

(8)   Proximity Probes

(9)   Drill bit
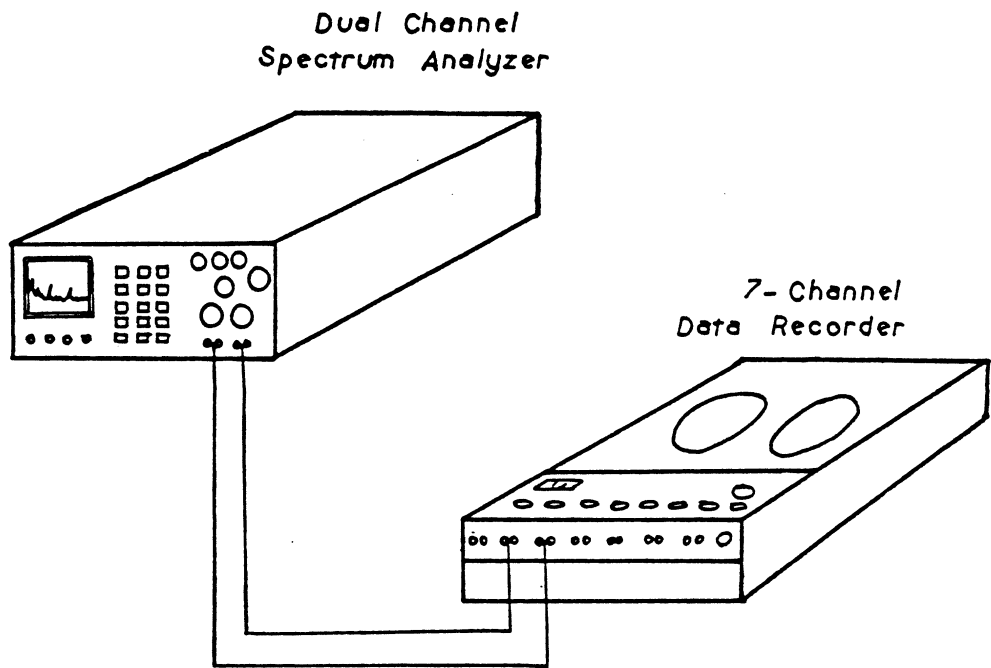
Fig. 2.2   Playback for spectrum analysis.
          Data recorder and Spectrum Analyzer.

D	L	f	Ω	T (1)	T (2)	T found	Fz (3)	Fz (4)	Fz (5)	Fz found
(mm)	(mm)	(mm/rev)	(rpm)	(N-m)	(N-m)	(N-m)	(N)	(N)	(N)	(N)
3.175	152.4	.0762	1800	0.428	0.722	0.271	184.	929.	411.	284.
4.762				0.880	1.353	0.789	276.	595.	515.	595.
6.350			650	1.466	2.233	1.883	369.	622.	667.	729.
			1300			1.827				675.
			1800			1.308				778.
			3600			1.042				729.
		.1524	1800	2.526	3.879	2.334	631.	1142.	951.	1142.
	304.8	.0762		1.466	2.233	1.184	369.	622.	667.	729.

Table 4.1   Torque and Trust measurements at various speeds and feeds compared with Boston's and Oxford's formulas.

D: drill diameter ; L: drill length ; T: torque

F_z: thrust ; w: web thickness ; c: chisel edge length

H_b: Brinell Hardness ; C_1, C_2, C_3: constants

(1) Boston's torque formula ; $T = K_1 f^{.78} D^{1.8}$

(2) Oxford's torque formula ; $T = K_2 H_b f^{.8} D^{1.8}$

(3) Torque found during experiments.

(4) Boston's first formula for trust ; $F_z = C_1 f^{.78} D$

(5) Boston's second formula for trust; $F_z = C_4 f^{.87} \{D/127 + w/D\}^{2.12}$

(6) Oxford's formula for trust ; $F_z = C_2 H_b f^{0.8} D^{0.8} + C_3 H_b c^2 D^2$

(7) Thrust found during experiments.

For the formula above refer to Appendix B.
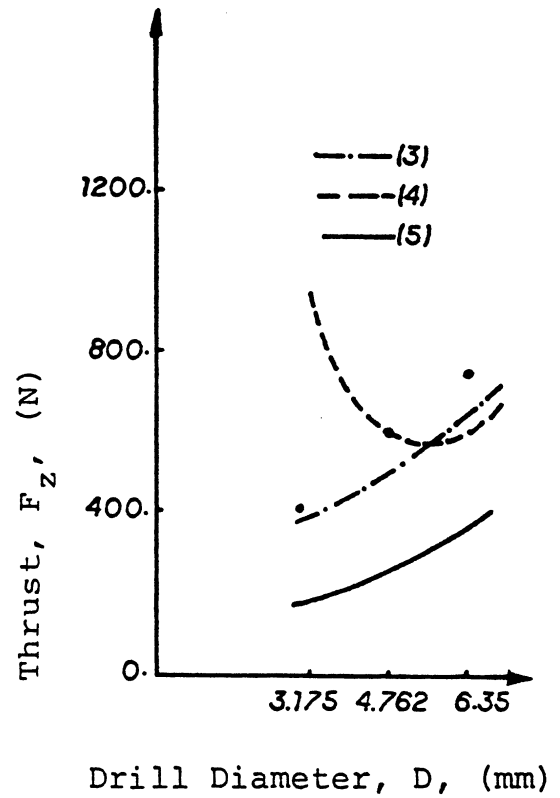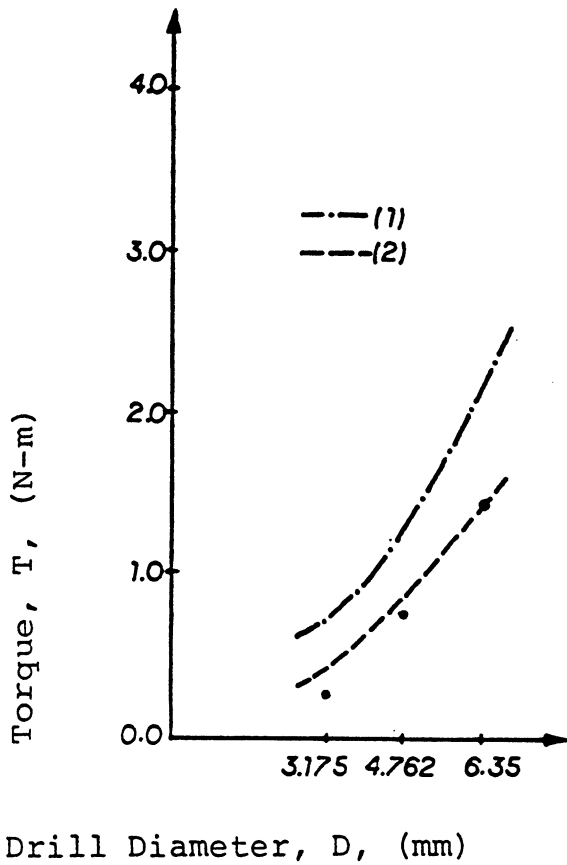
Fig. 4.2   Torque and Thrust vs. Drill Diameter while
           drilling AISI 1112 steel at 1800 rpm, compared
           with Boston's and Oxford's formulas. Feed:
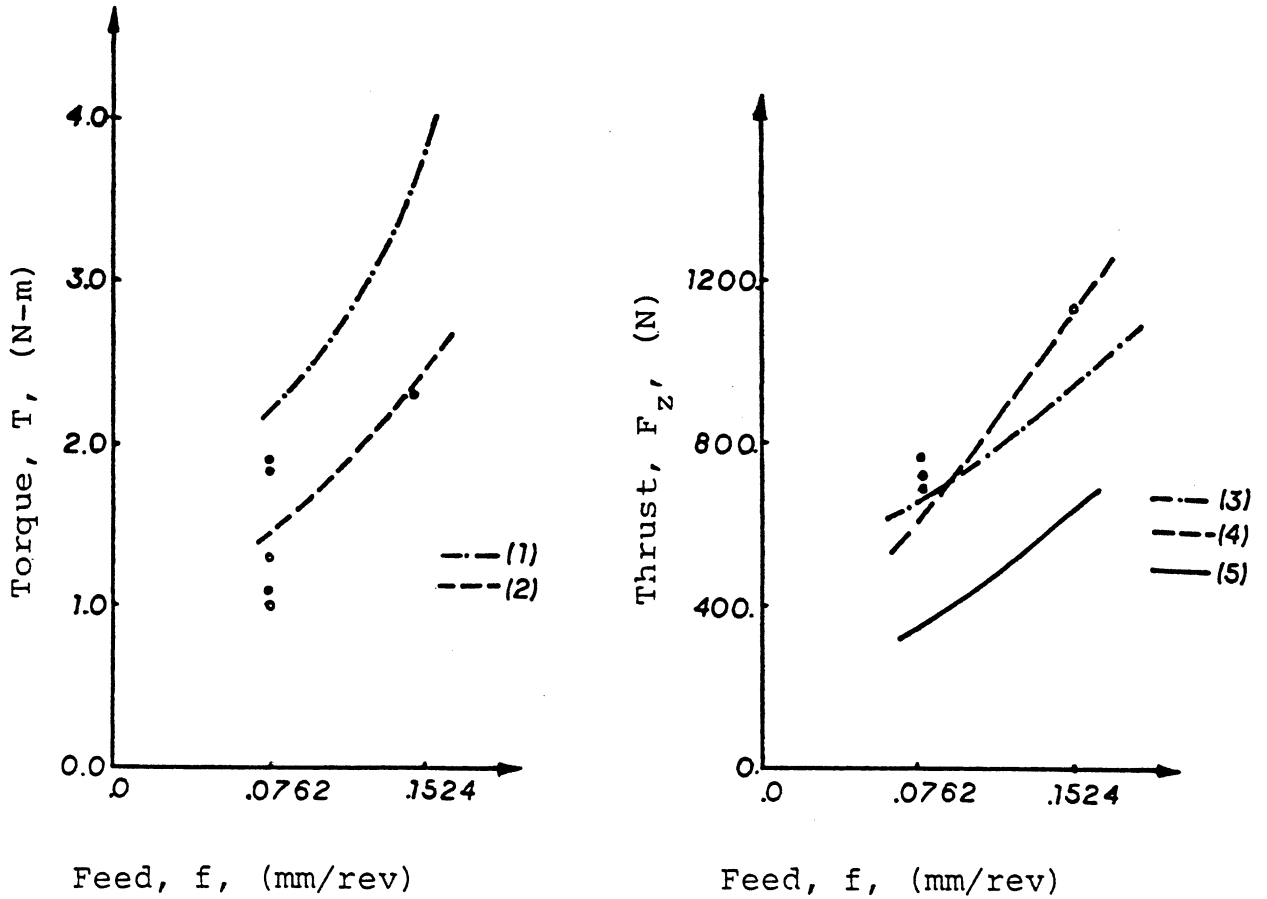   0.0762 mm/rev. For (1), (2), (3), (4), (5)
           refer to Fig. 4.1.

Fig. 4.1 Torque and Trust vs. feed at various rotational speeds while drilling AISI 1112 steel, compared with Boston's and Oxford's ·formulas.

(1) Oxford's torque formula, $T = K_2 \ H_b \ f^{0.8} \ D^{1.8}$

(2) Boston's torque formula, $T = K_1 \ f^{0.78} \ D^{1.8}$

(3) Oxford's formula for thrust, $F_z = C_2 \ H_b \ f^{0.8} \ D^{0.8} + C_3 \ H_b \ c^2$

(4) Boston's second formula for thrust $F_z = C_4 \ f^{0.87} \left(\dfrac{D}{127} + \dfrac{w}{D}\right)^{2.12}$

(5) Boston's first formula for thrust $F_z = C_1 \ f^{0.78} \ D$

For the formulas given ,above see also appendix B.
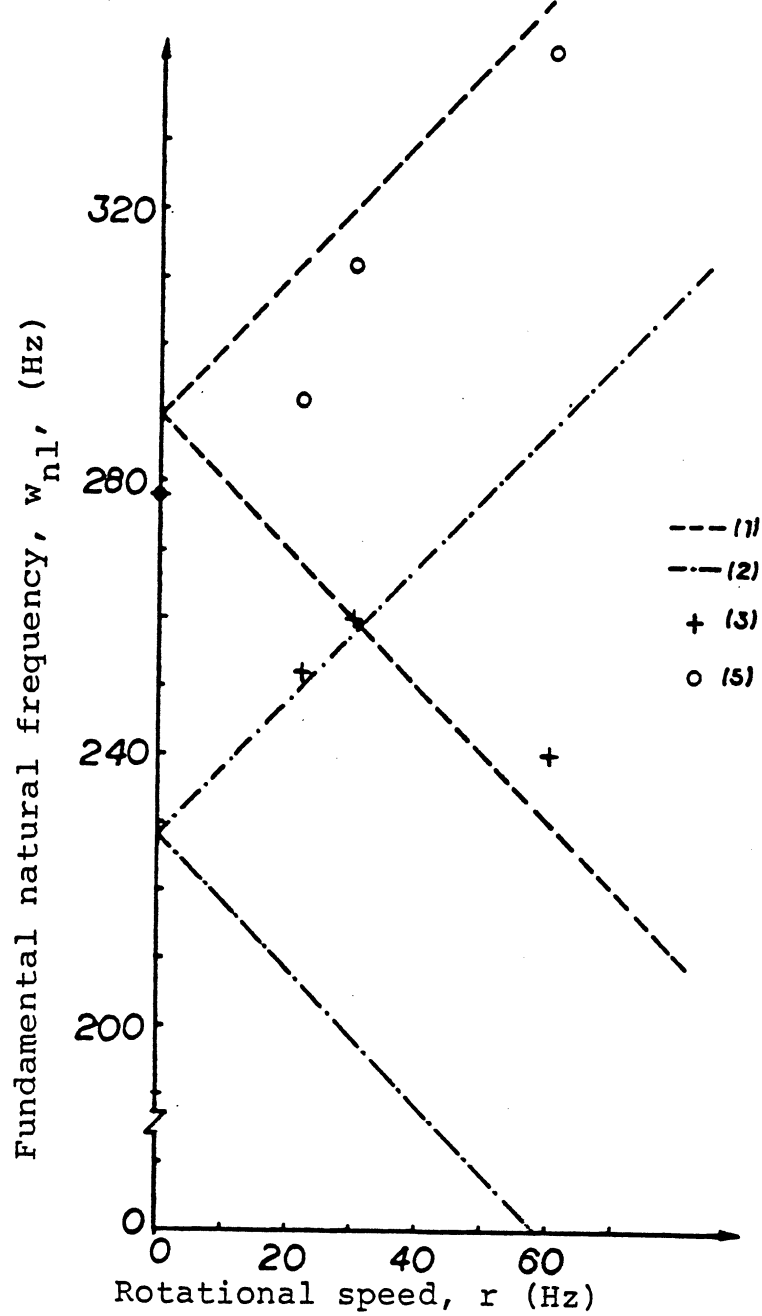
Fig. 4.3   The change in fundamental natural frequencies
           vs. drill rotational speed, model predictions
           and experimental data for:

           Drill diameter (D) = 6.35, Drill length ℓ = 304.8 mm,
           feed (f) = 0.0381 mm/rev.

           (1) Solid rod model

           (2) Fluted rod model

           (3) Upper fundamental natural frequency

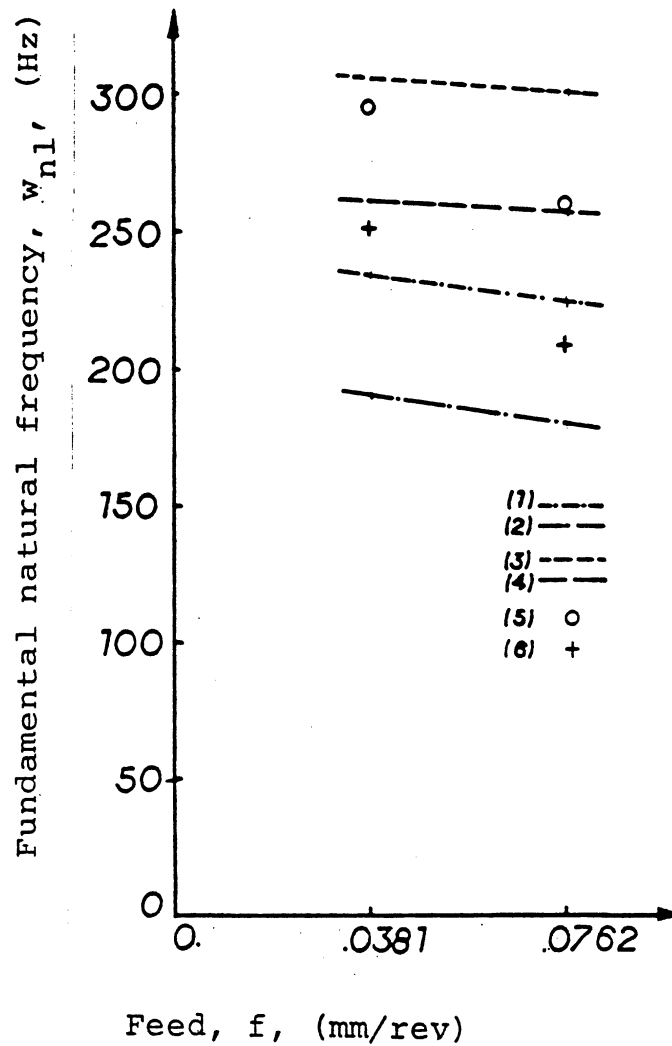   (4) Lower fundamental natural frequency

Fig. 4.4 Fundamental natural frequency at two different feeds. Model predictions and experimental data taken at approximately 12 mm depth. Drill length ℓ = 304.5 mm; Rotational speed: 22 Hz;

(1), (2) model predictions for fluted rod (upper and lower fundamental frequencies)

(3), (4) model predictions for solid rod (upper and lower fundamental frequencies)

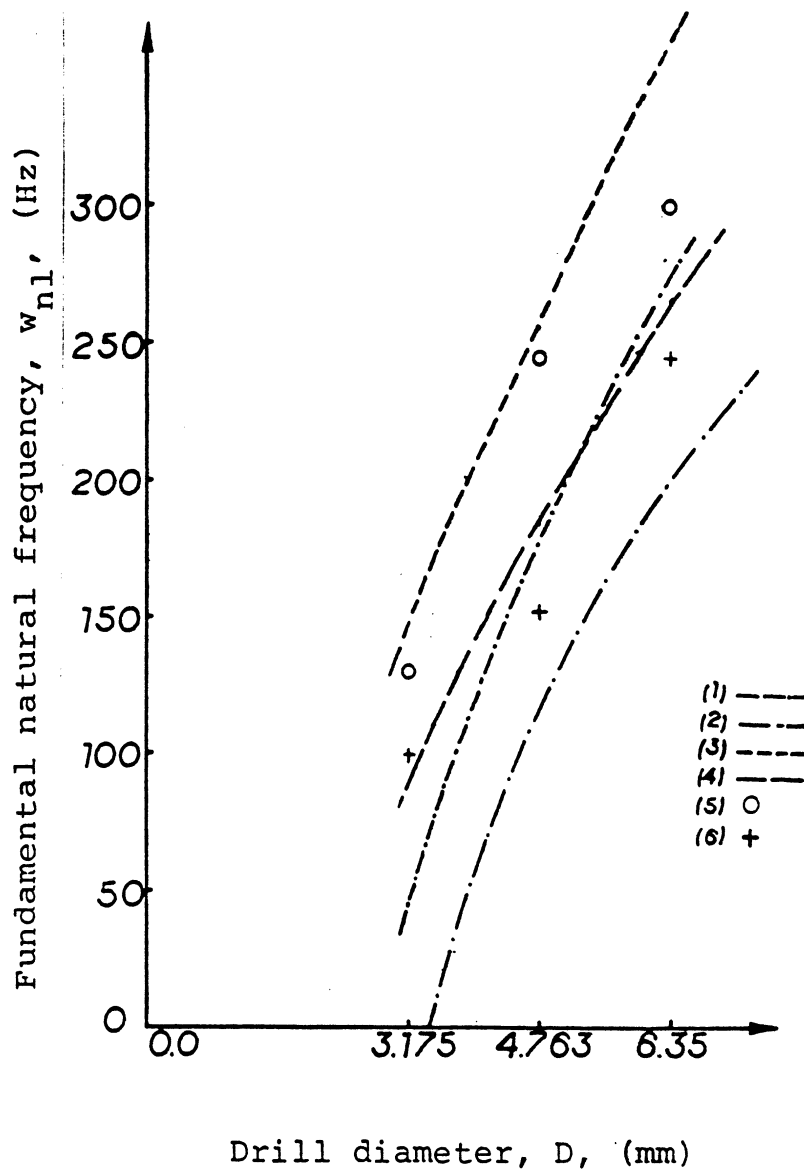(5), (6) upper and lower fundamental frequencies found experimentally.

Fig. 4.5 Drill diameter vs. fundamental natural frequencies at zero rotational speed where depth (d) is the parameter. Experimental foundings and model predictions. Drill length, ℓ = 304.5 mm.

(1) Fluted rod model, d = 40 mm.

(2) Fluted rod model, d = 5 mm.

(3) Solid rod model, d = 40 mm.

(4) Solid rod model, d = 5 mm.

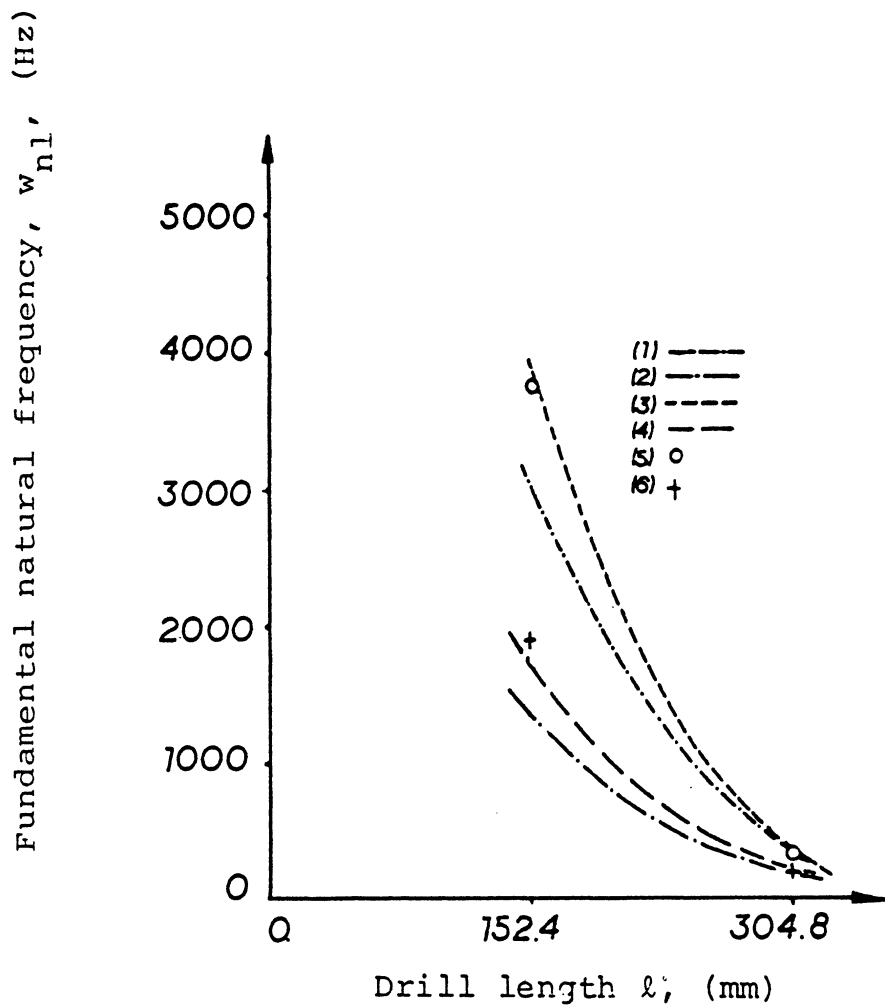(5) Experimental data, d = 40 mm.

(6) Experimental data, d = 5 mm.

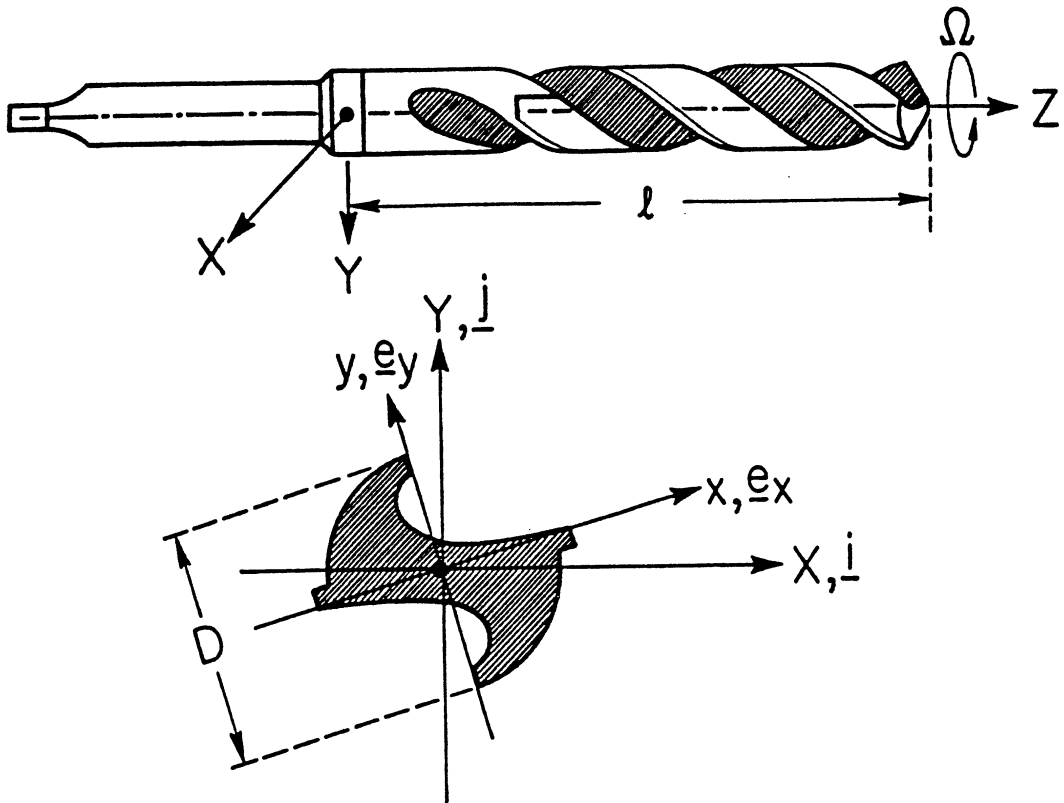Fig. 4.6 Drill length vs. fundamental natural frequencies
          at zero rotational speed where depth (d) is the
          parameter. Experimental foundings and model
          predictions. D = 6.35 mm.

(1) Fluted rod model, d = 40 mm.

(2) Fluted rod model, d = 5 mm.

(3) Solid rod model, d = 40 mm.

(4) Solid rod model, d = 5 mm.

(5) Experimental data, d = 40 mm.

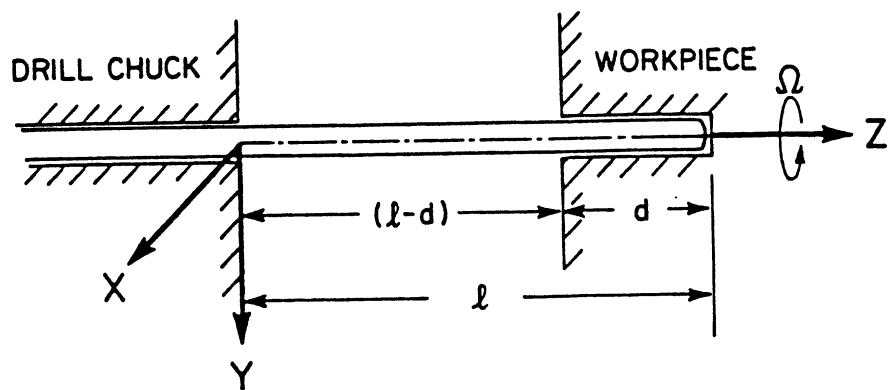(6) Experimental data, d = 5 mm.

Fig. A-1a. Drill geometry. [4]
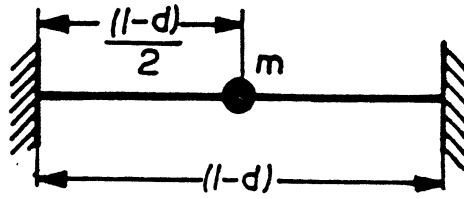

Fig. A-1b. Drill support conditions [4]
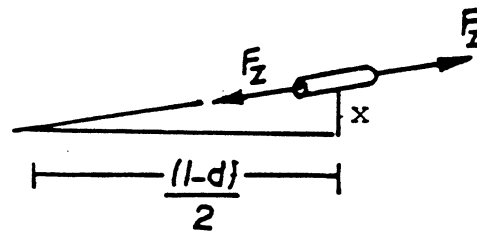
Fig. A-2 Mass lumped at the middle of massless rod.

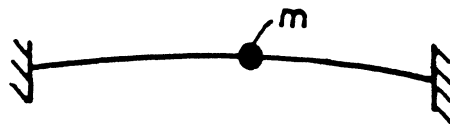
Fig. A-3 Effect of thrust force on the stiffness.

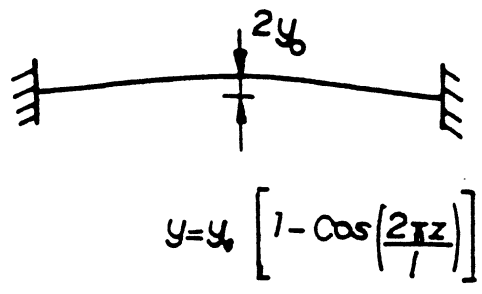$$y = y_0 \left[1 - \cos\left(\frac{2\pi z}{l}\right) \right]$$

Fig. A-4 First mode of the clamped damped beam and the
approximate curve [28],
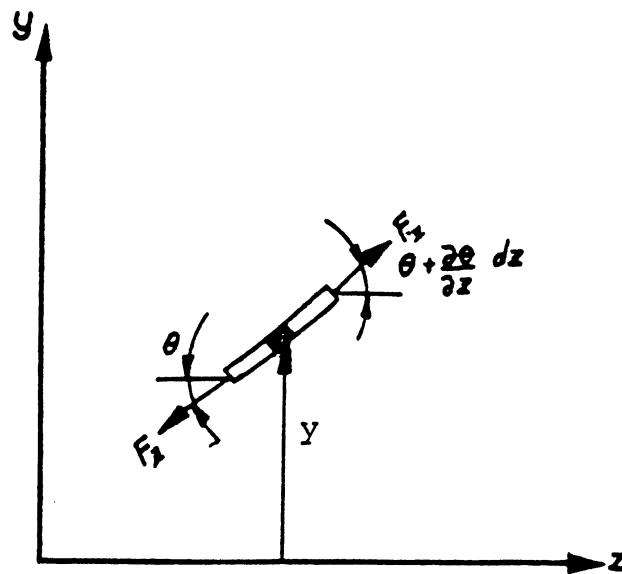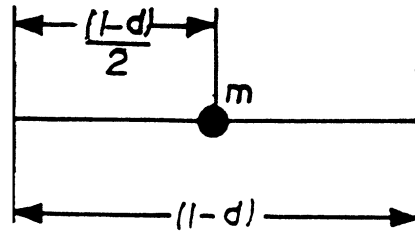
Fig. A-5   Mass lumped at the middle of the string
and the vibrating string differential element.

	α	β
Static formulation (A-14)	192.0	4.0
Equivalent mass formulation (A-21)	512.0	10.66
Equivalent stiffness formulation (A-30)	501.75	9.87

$$\omega_{nl} = \left(\frac{\alpha EI}{\rho A (\ell-d)^4} - \frac{\beta F_z}{\rho A (\ell-d)^2}\right)^{1/2}$$

Table A-1   Comparison between static, equivalent mass and equivalent stiffness formulations.

Parameter (Units)	Value
Ω (rad/s)	0.
ℓ (m)	0.259
D (m)	$6.35 \; 10^{-3}$
ρ (kg/m^3)	7850.
E (Pa)	200.10^9
d (m)	0.04
f (m/rev)	$7.62 \; 10^{-5}$
F_z (N)	755.
I_{xx}, I_{yy} (m^4)	$3.081 \; 10^{-11}$
A (m^2)	$1.967 \; 10^{-5}$

Table A-2   Parameters and the values used for the calculation of zero speed theoretical natural frequency of an experiment.

	Fundamental Transverse Natural Frequency, ω_{n1}, (Hz)
Experimental	298.
Static formulation	216.
Effective mass formulation	352.
Effective stiffness formulation	350.

Table A-3 Comparison between an experimental point and three theoretical formulation.